Hydrothermal synthesis of high refractive index thin films from chromium slag

Tong Sun[1,2], Lian-li Liu[3], Shu-ying Xu[1,2], Li-li Wang[3], Wei Li[1,2], Han Hao[1,2]

[1]*Key Laboratory of Applied Chemistry, Bohai University, Jinzhou 121013, People's Republic of China*
[2]*College of Chemistry, Chemical Engineering and Food Safety, Bohai University, Jinzhou 121013, People's Republic of China*
[3]*Liaoning Province Research Center for Silicon Materials Engineering Technology, Bohai University, Jinzhou 121013, People's Republic of China*
E-mail: jzsuntong@sina.com

Published in Micro & Nano Letters; Received on 10th June 2013; Revised on 23rd July 2013; Accepted on 26th July 2013

Chromium slag is a hazardous waste, and its high-value-added comprehensive utilisation would be advantageous. High refractive index thin films were prepared on glass substrates by a hydrothermal method from chromium slag with different mineralisers. The samples were characterised by inductively coupled plasma, X-ray diffraction, Fourier transform infrared spectroscopy, scanning electron microscopy, an atomic force microscope, a transmission electron microscope and by film thickness and refractive index. The results show that a few Fe_2O_3, FeOOH, Al_2O_3, AlOOH or MgO crystals are formed, and most compounds of iron, aluminium, magnesium and chromium are still in amorphous state. The film materials are combined with a glass substrate by a chemical bond. The coordination ability of mineraliser anion and metal ion affects the sediment reaction rates. With $NaClO_3$ or $NaHCO_3$ as a mineraliser, the film surface is a perfect three-dimensional space orientation network sediment with fine twines and small pores. The thinner the film, bigger the refractive index will be. The films' refractive index is mainly related to the film structure and non crystalline phase.

1. Introduction: In recent years, high refractive index materials have attracted wide attention because of their wide application for antireflection coatings, optical waveguides and optoelectronic devices [1–3]. Refractive index is an important evaluation criterion of the optical materials which can be applied to optics design and optical applications. The thickness and curvature of the component could be reduced by high index refractive materials, and the weight could be reduced at the same refractive. Hence, it could make the optical instrument light weight and miniaturised. Meanwhile, more researches of composited films with high refractive index were reported [1, 2, 4]. Common high refractive index materials are TiO_2 [5], ZrO_2 [6], ZnS [1, 7] and so on. The preparation methods of inorganic film mainly involved the sol–gel method [8, 9], hydrothermal method [10, 11], spin-coating methods [12, 13], chemical vapour deposition method [14, 15], spray pyrolysis method [16, 17], low temperature RF plasma treatment [18], the liquid phase deposition method [19] and so on. Of the above methods, the hydrothermal method was widely applied because of its mature technological conditions, simplicity of operation, moderate reaction conditions and uniformity of the coating film.

As a hazardous waste, chromium slag is harmful to the environment. In China, the accumulated amount of chromium slag is more than 6 million tons, and 200–300 thousand tons discharged annually. Most of the chromium slag is stacked on the ground, and its pollution is mainly controlled by biological treatment [20, 21], reduction method [22], cement solidification [23] and so on. However, there are few reports about the high-value-added comprehensive utilisation of chromium slag. There are more compounds of iron, aluminium, chromium, calcium and magnesium in chromium slag, and more functional products of iron, aluminium, chromium, calcium and magnesium are reported [24–28]. Hence, preparation of material with special performance is of great importance for the comprehensive use of chromium slag.

In this Letter, to prepare high-value-added production from chromium slag, high refractive index thin composited films were prepared on glass substrates from chromium slag by the hydrothermal method with different mineralisers. Characterisation of the samples was done using inductively coupled plasma (ICP), X-ray diffraction (XRD), Fourier transform infrared spectroscopy (FTIR), scanning electron microscopy (SEM) and a transmission electron microscope (TEM); meanwhile, the film thickness and refractive index were measured.

2. Experiment

2.1. Pretreatment of chromium slag: The chromium slag was crushed and dissolved in hydrochloric acid, and then the turbid solution was filtrated to dislodge the undissolved substance. To reduce hexavalent chromium, a saturated solution of ferrous sulphate was added into the filtrate and it was reacted for 30 min under stirring condition. After that, the above liquor's pH was adjusted to 3.5 by the sodium hydroxide solution. Then, the turbid liquid was filtrated after precipitating completely. The residue was dissolved by 3.0 mol/l hydrochloric acid, and the raw material liquid of the films was prepared.

2.2. Deposition of composite films: The thin composited films were deposited onto glass substrates by the hydrothermal method. 20 ml of the raw material liquid's pH was adjusted to 11.0 by sodium hydroxide, and 1 ml of 1 wt% polyethylene glycol 6000 solution and 5 ml of 0.01 mol/l mineraliser solution were added. Then, the solutions were each shifted into the hydrothermal reactors to 70% filling, and the microslides were placed vertically as glasses substrates. Afterwards, the reactors were sealed and heated at 160°C for 6 h. After the reactors were cooled naturally to room temperature, the glasses substrates were taken out and washed by deionised water and were then dried at 80°C. The powders were prepared simultaneously.

2.3. Characterisation of samples: The metal component content of the powders was analysed by ICP-OES (VISTA-MPX ICP-OES, VARIAN, America), which were prepared simultaneously with the composite films. The crystalline structure of the powders was determined by D/MAX-RB XRD (Rigaku, Japan) with Cu K-radiation in the 2θ range of 10°–80° at a scan rate of 4°/min. The FTIR of the powders was determined by a Scimitar 2000 Near FTIR spectrometer (Thermo electron, USA) and the spectra were recorded in the range of 4000–400 cm^{-1}. The morphologies

of the powders were examined by TEM (TEM, Philips EM400 T, Holland). The roughness of the films was measured by an AFM (AFM, Park System, Korea).

The surface morphologies of the films were examined by SEM (SEM, Shimadzu SSX-550 Japan). The films' thickness and reflective index at 632.8 nm were evaluated with an automatic elliptical polarisation thickness gauge (SGC-2, Tianjin, China).

3. Results and discussion

3.1. XRD analysis of the powders: The metallic element contents of the powders are given in Table 1 which were measured by ICP. Since all the results are similar, one of the results is shown.

The XRD spectra of the powders reveals that the phase structures of the samples are affected by the mineralisers, which were prepared simultaneously with the films (Fig. 1). With Na_2CO_3 and $NaHCO_3$ as the mineralisers, more $CaCO_3$ crystals are formed. It may be that CO_3^{2-} reacted with Ca^{2+} to form a $CaCO_3$ crystal in the hydrothermal process. However, the $CaCO_3$ crystal peaks are stronger with $NaHCO_3$ as the mineraliser than that of Na_2CO_3. This is due to more CO_3^{2-} of $NaHCO_3$ at the same mineraliser dose. The weak diffractive peaks of Fe_2O_3, FeOOH, Al_2O_3, AlOOH or MgO crystals appeared, and the kinds of crystals are affected by the mineraliser. There are weak peaks of Fe_2O_3, AlOOH and MgO crystals with Na_2CO_3 as the mineraliser, and there are weak peaks of FeOOH, Al_2O_3 and AlOOH crystals with Na_2HPO_4 or $NaClO_3$ as the mineraliser. Moreover, there are weak peaks of Fe_2O_3, AlOOH and MgO crystals when the mineraliser is $NaHCO_3$. The above results are caused by the different coordination ability of each mineraliser anion with metal ion. Table 1 shows that there is more iron and aluminium compound in the samples, nevertheless few crystals of these are formed. It demonstrates that most compounds of iron, aluminium, magnesium and chromium are still in amorphous state.

Table 1 Percentage composition of metallics in the powders

Metallic element	Fe_2O_3	Al_2O_3	CaO	Cr_2O_3	MgO	Na_2O	K_2O
wt%	30.46	12.26	5.27	5.83	13.71	2.98	0.97

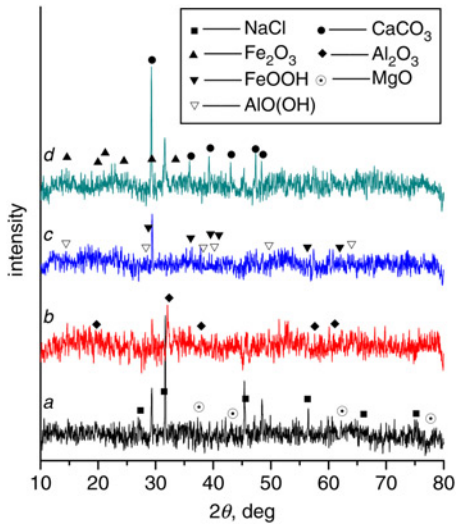

Figure 1 *XRD patterns of composited powders prepared with different mineralisers*
a Na_2CO_3
b Na_2HPO_4
c $NaClO_3$
d $NaHCO_3$

3.2. FTIR spectra analysis: Fig. 2 presents the FTIR spectra of the as-prepared powders with the films simultaneously. Both exhibit a strong absorption at 3500–3300 cm^{-1} for the stretching vibration of non-chemical bond association OH groups and 1645 cm^{-1} for H–O–H bending vibrations, indicating water adsorption [5]. Furthermore, the peaks at 1411, 872 and 716 cm^{-1} correspond to characteristic absorption peaks of $CaCO_3$crystal [29]. When the mineraliser is $NaHCO_3$, the peaks of the $CaCO_3$ crystal are stronger than the others, it means that the sample contains more $CaCO_3$ crystal, the result agrees with the XRD analysis.

The peaks at 1100 cm^{-1} are regarded as Si–O–Si asymmetrical stretching vibration, at 989 cm^{-1} they correspond to stretching vibration of Si–O–Fe, at 1022 cm^{-1} correspond to stretching vibration of Si–O–Al or Si–O–Mg [30, 31]. This indicates that the alkalinity groups have reacted with the glass substrate in the hydrothermal process, and the film sediment is combined with the glass substrate by chemical bond. Fig. 2 shows that the peaks of Si–O–Si are stronger with Na_2CO_3 or $NaHCO_3$ as a mineraliser, however the peaks of Si–O–Fe are stronger with the Na_2HPO_4 mineraliser and the peaks of Si–O–Al and Si–O–Mg are stronger with the $NaClO_3$ mineraliser. It demonstrates that CO_3^{2-} is favourable for Si–O–Si, HPO_4^{2-} is favourable for Si–O–Fe and ClO_3^- is favourable for Si–O–Al and Si–O–Mg bands. This may be because of the different coordination abilities of the mineraliser anion and metal ion.

The peaks at 672 and 420 cm^{-1} are attributed to flexural vibrations of Fe–OH, at 603 cm^{-1} they are the characteristic absorption peaks of Al–OH and Mg–OH flexural vibrations, and the peaks at 467 cm^{-1} are for Fe–O [32, 33]. Fig. 2 shows that the aforesaid peaks are weakest when the mineraliser is Na_2CO_3, indicating that HPO_4^{2-} or ClO_3^- is favourable for the above chemical bonds formation. Meanwhile, a high concentration of free CO_3^{2-} is favourable for the above chemical bonds formation.

3.3. SEM microphotographs analysis and roughness of the composite films: SEM micrograph images of the films show that the film surface morphologies are affected by the mineraliser

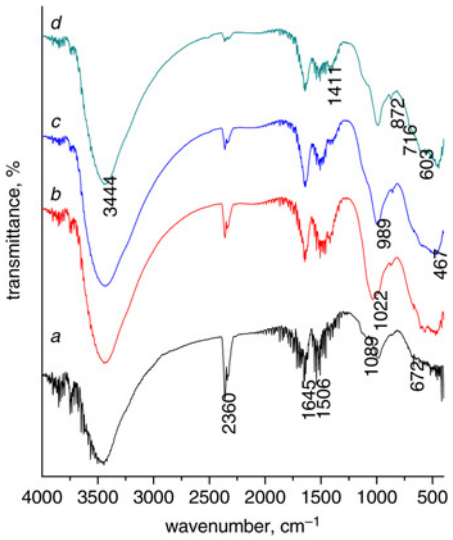

Figure 2 *FTIR spectra of the samples prepared with different mineralisers*
a Na_2CO_3
b Na_2HPO_4
c $NaClO_3$
d $NaHCO_3$

doi: 10.1049/mnl.2013.0373

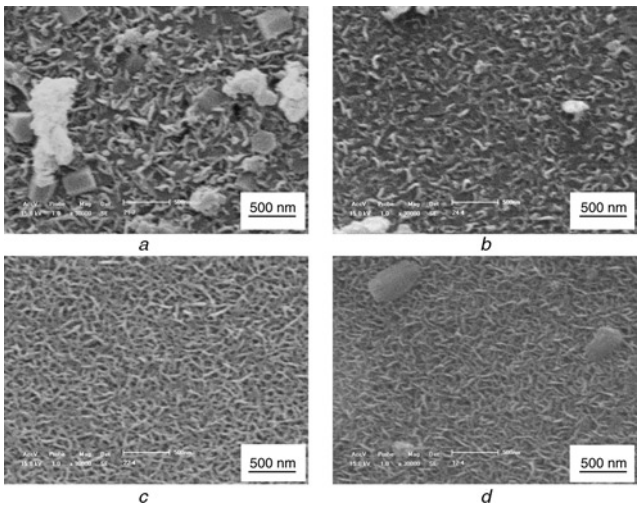

Figure 3 *SEM images of composited films prepared with different mineralisers*
a Na_2CO_3
b Na_2HPO_4
c $NaClO_3$
d $NaHCO_3$

(Fig. 3). With Na_2CO_3 as the mineraliser, there are more big particles and uneven flake sediments on the film surface. When the mineraliser is Na_2HPO_4, more uneven flake sediments are formed. However, with $NaClO_3$ or $NaHCO_3$ as the mineraliser, the film surface is covered by a perfect three-dimensional (3D) network sediment with fine twines and small pores.

Furthermore, the average roughness (Ra) of the composite films is 31.250, 20.727, 25.270 and 22.248 nm, respectively, when the mineraliser is Na_2CO_3, Na_2HPO_4, $NaClO_3$ or $NaHCO_3$. It is shown that the Ra of the composite films is related to the surface morphologies.

3.4. TEM microphotographs analysis of the powders: Fig. 4 shows the TEM images of the powders prepared simultaneously with the films. When the mineraliser is Na_2CO_3, nanometre particles agglomeration is observed. With Na_2HPO_4 as the mineraliser, the particles are aggregated regularly to form polyhedra. When the mineraliser is $NaClO_3$ or $NaHCO_3$, the powders are irregular minisize particles, and they are reunited slightly.

SEM and TEM results indicate that the structure of the film surface sediments is affected by the mineraliser anion. The mineraliser anions exist in the hydrothermal system of pH 11 in a different form. With Na_2CO_3 and $NaHCO_3$ as the mineralisers, the mineraliser anions are presented as CO_3^{2-}. Many metal ions and CO_3^{2-} form a coordination complex, and the concentration of the free metal ion is decreased, therefore the deposition reaction has slowed. In the hydrothermal system of the $NaHCO_3$ mineraliser, the concentration of CO_3^{2-} is greater than that of Na_2CO_3, and the deposition reaction is slower. Therefore a slower sedimentation velocity leads to good particle dispersions and a compact network structure of the film surface. Meanwhile, with Na_2HPO_4 as the mineraliser, the mineraliser anions are mainly presented as HPO_4^{2-} at pH of 11, but only a minor amount of PO_4^{3-} is presented. Hence, a little coordination complex of PO_4^{3-} and metal is formed, and most of the metal ions are free. This makes for acceleration of the hydrothermal reaction. Hence, more uneven flake particles are formed, and the film surface is coarse. When the mineraliser is $NaClO_3$, the mineraliser anions are presented as ClO_3^-, and a more coordination complex of ClO_3^- and metal ion leads to slowing of sediment reaction, hence the film surface appears as a compact network structure.

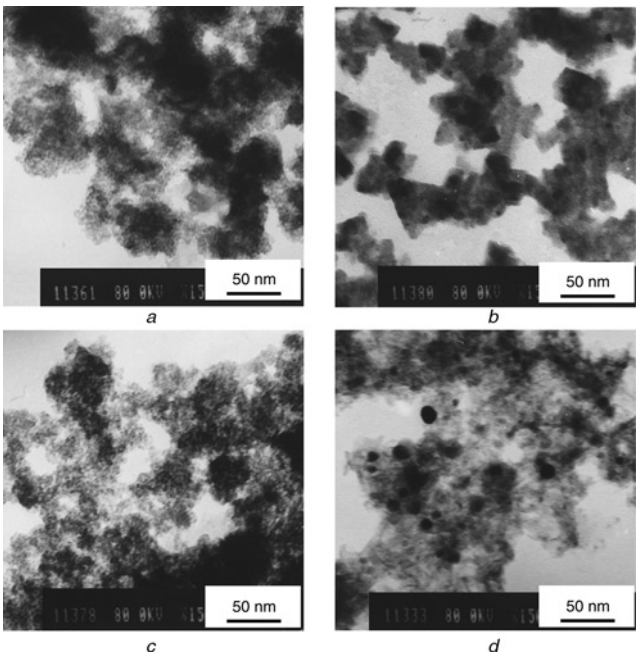

Figure 4 *TEM microphotographs of the composited powders prepared with different mineralisers*
a Na_2CO_3
b Na_2HPO_4
c $NaClO_3$
d $NaHCO_3$

3.5. Thickness and refractive index of the films: The thickness and refractive index of the films at 632.8 nm show that thinner the film is, the bigger the refractive index will be (shown in Fig. 5).

The refractive index commonly relates to film compactness and crystalline phase [31, 34]. Therefore taken together with the characterisation results, the mineraliser affects the film refractive index. With Na_2CO_3 as the mineraliser, more big particles and uneven flake sediments on the film surface lead to poor film compactness and severe scattering loss, so its refractive index is the minimum. Meanwhile, the thickest film probably could be attributed to big sediments velocity and uneven sediments on the film surface. With Na_2HPO_4 as the mineraliser, more uneven flake sediments and no big particles lead to ameliorative compactness, so the thickness of the film decreases but the refractive index does not increase. When the mineraliser is $NaClO_3$ or $NaHCO_3$, a low sediment velocity leads to a compact 3D network structure formation, hence

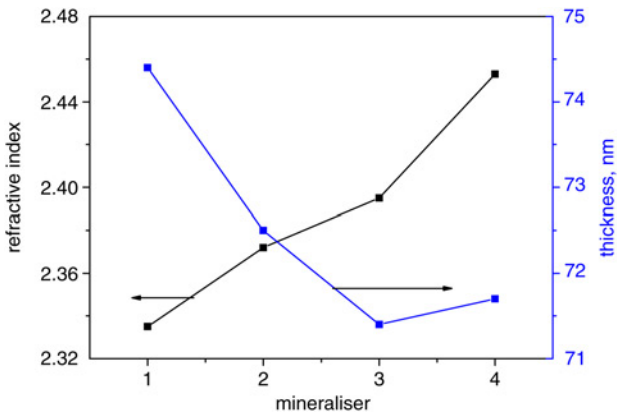

Figure 5 *Film thickness and refractive index of composited films prepared with different mineralisers*
(1) Na_2CO_3; (2) Na_2HPO_4; (3) $NaClO_3$; and (4) $NaHCO_3$

the films are thin. Meanwhile, small pores on the film surface cause slight scattering loss, and its refractive indices are high. With $NaHCO_3$ as the mineraliser, the twines are the thinnest and the pores are the smallest, the biggest refractive index may be because of the densest film. However, all the results show that the refractive indices of the films relate to the film structure and non-crystalline phase; this could probably affect the extent of the film structure which is greater than that of the crystalline phase.

4. Conclusions: High refractive index films were deposited on glass substrates from chromium slag by the hydrothermal method with different mineralisers. A few Fe_2O_3, FeOOH, Al_2O_3, AlOOH or MgO crystals are formed, and most compounds of iron, aluminium, magnesium and chromium are still in the amorphous state. The FTIR results show that the alkalinity group has reacted with the glass substrate in the hydrothermal process, and the film material combines with the glass substrate by chemical bond. The coordination ability of the mineraliser anion and metal ion affects the sediment reaction rates. With $NaClO_3$ or $NaHCO_3$ as a mineraliser, the film surface is covered by a perfect 3D space orientation network sediment with fine twines and small pores. The thinner the film is, the bigger the refractive index will be. The films' refractive index is mainly influenced by the film surface structure.

5. Acknowledgments: The authors acknowledge financial support by the Institution of Higher Learning Innovative Teams of Liaoning (LT2012020) and the Project of Building Program for the Engineering Technology Research Center in Liaoning Province Science and Technology Agency (2009402007).

6 References

[1] Lü C., Cui Z., Wang Y., *ET AL.*: 'Preparation and characterization of ZnS–polymer nanocomposite films with high refractive index', *J. Mater. Chem.*, 2003, **13**, pp. 2189–2195

[2] Oubaha M., Elmaghrum S., Copperwhite R., Corcoran B., McDonagh C., Gorin A.: 'Optical properties of high refractive index thin films processed at low-temperature', *Opt. Mater.*, 2012, **34**, pp. 1366–1370

[3] Choi Y.-O., Kim N.-H., Park J.-S., Lee W.-S.: 'Influences of thickness-uniformity and surface morphology on the electrical and optical properties of sputtered CdTe thin films for large-area II–VI semiconductor heterostructured solar cells', *Mat. Sci. Eng. B, Solid.*, 2010, **171**, pp. 73–78

[4] Kim J.-H.: 'High refractive index nanocomposite cover-layer for optical storage media', *Opt. Mater.*, 2011, **33**, pp. 1185–1189

[5] Liu B.-T., Tang S.-J., Yu Y.-Y., Lin S.-H.: 'High-refractive-index polymer/inorganic hybrid films containing high TiO_2 contents', *Colloid. Surf. A*, 2011, **377**, pp. 138–143

[6] Inoue H., Watanabe Y., Masuno A., Kaneko M., Yu J.: 'Effect of substituting Al_2O_3 and ZrO_2 on thermal and optical properties of high refractive index La_2O_3–TiO_2 glass system prepared by containerless processing', *Opt. Mater.*, 2011, **33**, pp. 1853–1857

[7] Luo J., Qu D., Tikhonov A., Bohn J., Asher S.A.: 'Monodisperse, high refractive index, highly charged ZnS colloids self assemble into crystalline colloidal arrays', *J. Colloid. Interf. Sci.*, 2010, **345**, pp. 131–137

[8] Goktas A., Aslan F., Yasar E., Mutlu I.H.: 'Preparation and characterisation of thickness dependent nano-structured ZnS thin films by sol–gel technique', *J. Mater. Sci. Mater. Eng.*, 2011, **23**, pp. 1361–1366

[9] Chang C.-C., Cheng L.-P., Lin C.-Y., Yu Y.-Y.: 'Preparation and characterization of TiO_2 sols and their UV-cured hybrid thin films on plastic substrates', *J. Sol-Gel Sci. Technol.*, 2012, **63**, pp. 30–35

[10] Sahoo T., Jeon J.-W., Kannan V., *ET AL.*: 'Hydrothermal growth and characterization of ZnO thin film on sapphire (0001) substrate with p-GaN buffer layer', *Thin Solid Films*, 2008, **516**, pp. 8244–8247

[11] Chan P.-H., Lu F.-H.: 'Low-temperature hydrothermal–galvanic couple synthesis of $BaTiO_3$ thin films on Ti-coated silicon substrates', *Thin Solid Films*, 2009, **517**, pp. 4782–4785

[12] Kim S.-G., Hagura N., Iskandar F., Yabuki A., Okuyama K.: 'Multilayer film deposition of Ag and SiO_2 nanoparticles using a spin coating process', *Thin Solid Films*, 2008, **516**, pp. 8721–8725

[13] Merdes S., Kinoshita A., Hadjoub Z., *ET AL.*: 'Effect of alternating Cu poor/Cu rich/Cu poor/Cu rich/ layers of metal naphthenates in the growth process on the properties of $CuInSe_2$ thin films prepared by the spin coating technique', *Thin Solid Films*, 2008, **516**, pp. 7335–7339

[14] Thom K.M., Ekerdt J.G.: 'The effect of an iodine source on nucleation and film properties of Ru films deposited by chemical vapor deposition', *Thin Solid Films*, 2009, **518**, pp. 36–42

[15] Barve S.A., Jagannath, Mithal N., *ET AL.*: 'Effects of precursor evaporation temperature on the properties of the yttrium oxide thin films deposited by microwave electron cyclotron resonance plasma assisted metal organic chemical vapor deposition', *Thin Solid Films*, 2011, **519**, pp. 3011–3020

[16] Sirbu D., Rambu A.P., Rusu G.I.: 'Microstructure, wettability and optical characteristics of ZnO/In_2O_3 thin films', *Mat. Sci. Eng. B, Solid.*, 2011, **176**, pp. 266–270

[17] Suslov A., Lama P., Dorsinville R.: 'Fabrication and characterisation of nanostructured thin films of Ag synthesised using condensation on ion centres in gas', *Micro Nano Lett.*, 2011, **6**, pp. 955–957

[18] Dhayal M., Jun J., Gu H.B., Hee Park K.: 'Surface chemistry and optical property of TiO_2 thin films treated by low-pressure plasma', *J. Solid State Chem.*, 2007, **180**, pp. 2696–2701

[19] Lei C.X., Zhou H., Feng Z.D., Zhu Y.F., Du R.G.: 'Liquid phase deposition (LPD) of TiO_2 thin films as photoanodes for cathodic protection of stainless steel', *J. Alloy Compd.*, 2012, **513**, pp. 552–558

[20] Quan X., Tan H., Zhao Y., Hu Y.: 'Detoxification of chromium slag by chromate resistant bacteria', *J. Hazard. Mater.*, 2006, **137**, pp. 836–841

[21] Wu C., Zhang H., He P., Shao L.: 'Thermal stabilization of chromium slag by sewage sludge: effects of sludge quantity and temperature', *J. Environ. Sci.*, 2010, **22**, pp. 1110–1115

[22] Shi Y.-M., Du X.-H., Meng Q.-j., Song S.-W., Sui Z.-T.: 'Reaction process of chromium slag reduced by industrial waste in solid phase', *J. Iron Steel Res. Int.*, 2007, **14**, pp. 12–15

[23] Laforest G., Duchesne J.: 'Immobilization of chromium (VI) evaluated by binding isotherms for ground granulated blast furnace slag and ordinary Portland cement', *Cement. Concrete. Res.*, 2005, **35**, pp. 2322–2332

[24] Katiyar P., Jin C., Narayan R.J.: 'Electrical properties of amorphous aluminum oxide thin films', *Acta Mater.*, 2005, **53**, pp. 2617–2622

[25] Gupta R.K., Ghosh K., Kahol P.K.: 'Vertical exchange bias effects in multilayer thin films based on iron oxide and chromium oxide', *Mater. Lett.*, 2011, **65**, pp. 2429–2431

[26] Hassan S.F.: 'Effect of primary processing techniques on the microstructure and mechanical properties of nano-Y_2O_3 reinforced magnesium nanocomposites', *Mat. Sci. Eng. A, Struct.*, 2011, **528**, pp. 5484–5490

[27] Neri G., Bonavita A., Ipsale S., *ET AL.*: 'Pd- and Ca-doped iron oxide for ethanol vapor sensing', *Mat. Sci. Eng. B, Solid.*, 2007, **139**, pp. 41–47

[28] Belle C.J., Bonamin A., Simon U., *ET AL.*: 'Size dependent gas sensing properties of spinel iron oxide nanoparticles', *Sensor. Actuators B, Chem.*, 2011, **160**, pp. 942–950

[29] Gago-Duport L., Briones M., Rodriguez J., Covelo B.: 'Amorphous calcium carbonate biomineralization in the earthworm's calciferous gland: pathways to the formation of crystalline phases', *J. Struct. Biol.*, 2008, **162**, pp. 422–435

[30] Liu Y., Lü C., Li M., Zhang L., Yang B.: 'High refractive index organic–inorganic hybrid coatings with TiO_2 nanocrystals', *Colloid Surf. A*, 2008, **328**, pp. 67–72

[31] Wang F., Luo Z., Qing S., Qiu Q., Li R.: 'Sol–gel derived titania hybrid thin films with high refractive index', *J. Aalloy Compd.*, 2009, **486**, pp. 521–526

[32] Zeng Y., Park J.: 'Characterization and coagulation performance of a novel inorganic polymer coagulant – poly-zinc-silicate-sulfate', *Colloid Surf. A*, 2009, **334**, pp. 147–154

[33] Sun T., Liu L.L., Wang L.L., Zhang Y.P.: 'Preparation of a novel inorganic polymer coagulant from oil shale ash', *J. Hazard Mater.*, 2011, **185**, pp. 1264–1272

[34] Torres-Huerta A.M., Domínguez-Crespo M.A., Onofre-Bustamante E., Flores-Vela A.: 'Characterization of ZrO_2 thin films deposited by MOCVD as ceramic coatings', *J. Mater. Sci.*, 2011, **47**, pp. 2300–2309

doi: 10.1049/mnl.2013.0373